

1 **Measurement of the Seebeck coefficient under high**  
2 **pressure by dual heating**

3

4 Takashi Yoshino<sup>1\*</sup>, Ran Wang<sup>1</sup>, Hitoshi Gomi<sup>1,2</sup>, Yoshihisa Mori<sup>3</sup>

5 <sup>1</sup>Institute for Planetary Materials, Okayama University, Misasa, Tottori 682-0193, Japan

6 <sup>2</sup>Earth and Life Science Institute, Tokyo Institute of Technology, Tokyo 152-8550,

7 Japan

8 <sup>3</sup>Department of Applied Science, Okayama University of Science, Ridai 1-1, Kita-ku,

9 Okayama 700-0005, Japan

10

11 \*Corresponding author. Tel: +81-0858-43-3737; Fax: +81-0858-43-2184.

12 E-mail address: tyoshino@misasa.okayama-u.ac.jp

13

14 **Abstract**

15 This study presents a new method for measuring the Seebeck coefficient under high  
16 pressure in a multi-anvil apparatus. The application of a dual-heating system enables  
17 precise control of the temperature difference between both ends of the sample in a high-  
18 pressure environment. Two pairs of W-Re thermocouples were employed at both ends  
19 of the sample to monitor and control the temperature difference, and independent probes  
20 were arranged to monitor the electronic motivate force (emf) produced by temperature  
21 oscillation at a given target temperature. The temperature difference was controlled  
22 within 1 K during the resistivity measurements to eliminate the influence of emf owing  
23 to a sample temperature gradient. The Seebeck measurement was successfully measured  
24 from room temperature to 1400 K and obtained by averaging two measured values with  
25 opposite thermal gradient directions (~20 K). Thermoelectric properties were measured  
26 on disk-shaped p-type Si wafers with two different carrier concentrations as a reference  
27 for high Seebeck coefficients. This method is effective to determine the thermoelectric  
28 power of materials under pressure.

29

30 **I. INTRODUCTION**

31 The application of pressure to thermoelectric materials produces interesting  
32 property changes.<sup>1-5</sup> Knowledge of thermoelectric properties at high pressures is  
33 therefore important for understanding not only pressure tuning of thermoelectric  
34 conversion materials to improve transport properties, but also the electromagnetic  
35 behavior of materials in the Earth's interior. The Seebeck coefficient describes the

36 voltage ( $\Delta V$ ) that develops from a given temperature difference ( $\Delta T$ ) in a material ( $S =$   
37  $\Delta V/\Delta T$ ). The Seebeck coefficient ( $S$ ) is an integral part of the heat-to-electricity  
38 conversion in thermoelectric devices, given by  $zT = S^2\sigma T/\kappa$ , where  $\sigma$  is electrical  
39 conductivity,  $\kappa$  is thermal conductivity,  $T$  is temperature, and  $z$  is thermoelectric figure  
40 of merit. Previous theoretical and experimental studies have suggested that particularly  
41 high  $zT$  magnitudes can be obtained in existing thermoelectric materials (e.g., PbTe,  
42 PbSe, Bi<sub>2</sub>Te<sub>3</sub>) at high pressure.<sup>6-9</sup>

43       The Seebeck coefficient is an important parameter to identify the type of electric  
44 charge carrier in a semiconductor. Although a good thermoelectric material should have  
45 only one dominant type of charge carrier type, the Earth's constituent minerals have  
46 thermoelectric contributions from both n- and p-type carriers. For example, the  
47 thermopower of olivine, the dominant mineral in the upper mantle, shows a gradual  
48 change across zero with increasing temperature, suggesting a transition from polaron  
49 dominance in conduction to magnesium vacancy dominance around 1573K.<sup>10,11</sup> Some  
50 thermal boundary layers are known to exist in the Earth's interior (e.g., core-mantle  
51 boundary). Large temperature gradients may affect the redox state of the Earth's deep  
52 interior by the Seebeck effect, which makes knowledge of the electrical charge polarity  
53 in constituent minerals required for understanding the redox evolution of the mantle.  
54 However, Seebeck coefficient measurements at pressures relevant to the Earth's mantle  
55 remains unreported.

56       Seebeck coefficient measurements under pressure have progressed using a  
57 Bridgman-type high-pressure apparatus at room temperature, but most recent studies

58 have involved a diamond anvil cell (DAC) .<sup>4,5,12-14</sup> However, DAC studies may involve  
59 uncertainties in the determined properties of bulk materials owing to the small sample  
60 size and unstable heating at high temperature. In contrast, thermoelectric measurements  
61 in a multi-anvil apparatus allow substantially larger samples and more stable heating.  
62 Several studies have therefore determined the electrical conductivity of mantle minerals  
63 up to 25 GPa and 2000 K using in situ complex impedance spectroscopy in a Kawai-  
64 type multi-anvil high pressure apparatus.<sup>15</sup> Thermal conductivity or diffusivity under  
65 simultaneously high temperatures and pressures have also been measured using impulse  
66 heating methods in a Kawai-type multi-anvil press.<sup>16</sup> However, measurements of the  
67 Seebeck coefficient in a multi-anvil apparatus at high pressure remain scarce. A high-  
68 pressure setup for performing the simultaneous determination of diffusivity and  
69 Seebeck coefficient in a multi-anvil apparatus at room temperature was first reported by  
70 Jacobsen et al.<sup>17</sup> Yuan et al.<sup>18</sup> developed a method for simultaneously measuring  
71 electrical resistivity and the Seebeck coefficient at high pressure (5 GPa) and  
72 temperatures up to 750 K in a cubic multi-anvil apparatus. This method uses the  
73 inherent temperature gradient in samples along the axial direction of the cylindrical  
74 heater, which is essential for measuring the Seebeck coefficient. The  $\Delta T$  between both  
75 sample ends in a high-pressure cell tends to increase with increasing average sample  
76 temperature. Large uncertainties are often unavoidable at high temperature because the  
77 thermoelectromotive force (emf) of the semi-conducting materials themselves is  
78 typically non-linear with  $\Delta T$ . Alternatively, installation of an additional heater can be  
79 useful to control small  $\Delta T$  between sample ends during thermoelectric power

80 measurements to allow accurate determination of the Seebeck coefficient near the target  
81 temperature.

82 For this purpose, we have developed a dual-heating system for accurate  $\Delta T$  control  
83 between both ends of the sample in the 6-axis press installed at Institute for Planetary  
84 Materials, Okayama University. Because a Kawai-type (6-8) multi-anvil press can  
85 generate much higher pressures than a cubic multi-anvil press, we developed an  
86 octahedron cell including dual heaters. We introduce the system specifications and  
87 performance with technical and analytical protocols to determine the Seebeck  
88 coefficient under high temperature and pressure conditions. This method is useful to  
89 determine the thermoelectric properties of conductive materials as a function of  
90 temperature at high pressure.

91

## 92 **II. EXPERIMENTAL METHOD**

### 93 **A. Principle of Seebeck coefficient measurement by dual heating**

94 Measurement of the Seebeck coefficient in materials only requires knowledge of  
95 the temperature difference and voltage across two locations on the sample. The  $\Delta T$  and  
96 electric potential are measured from probes in direct contact with the sample ends, and  
97 the Seebeck coefficient can be determined from the slope of  $\Delta V$  vs.  $\Delta T$  following the  
98 differential method.<sup>19</sup> Figure 1 shows a schematic design of the Seebeck coefficient  
99 measurement used in our laboratory. The probes serve as both two sets of  
100 thermocouples and voltage leads from both ends of the sample. The thermocouples are  
101 not involved in the emf measurement. Each thermocouple is connected to each side of a

102 disk-shaped sample through a metal electrode. Each of the dual-heating systems is  
103 configured as a separate circuit from the thermopower measurement circuit. An AC  
104 power supply was used for heating. Proportional-integral-differential (PID) temperature  
105 control was used to generate  $\Delta T$  between both ends of the sample. Each heater controls  
106 the temperature at the position of the thermocouple to which it is closer located. The  $\Delta V$   
107 is measured at fixed pressure and variable  $\Delta T$ . The  $\Delta V$  values are measured and plotted  
108 to eliminate any voltage offset.<sup>20</sup> The Seebeck coefficient ( $S$ ) is calculated from the  
109 slope of the temperature difference ( $\Delta T = T_1 - T_2$ ) and emf ( $\Delta V$ ) assuming linearity in  $S$   
110 for the bulk sample. The absolute Seebeck coefficient is corrected for contributions of  
111 voltage from the contact wires by subtracting the Seebeck voltage produced by the  
112 probe wires. In the case of the semiconductor samples with particularly larger Seebeck  
113 coefficients ( $> 100 \mu\text{V/K}$ ), however, the small emf produced by the metal leads and WC  
114 anvils ( $\sim 1 \mu\text{V/K}$ ) can be ignored.

115

## 116 **B. Electrical resistivity measurement**

117 A four-wire resistance measurement design was used to measure the temperature-  
118 dependence of sample electrical resistivity. In the resistivity measurement, the  
119 temperature is controlled to be the same at both ends of the sample to avoid the  
120 thermopower derived from the sample itself. The obtained resistance data were  
121 processed to compute sample resistivity using Ohm's law,  $R = \frac{V}{I}$ , where  $R$  is resistance,  
122  $V$  is the voltage drop, and  $I$  is current. The sample resistivity was calculated on the basis

123 of the sample dimension  $\rho = \frac{RA}{L}$  where  $L$  and  $A$  are the sample length and cross-  
124 sectional area, respectively.

125

### 126 **C. Sample and Cell Assembly**

127 The samples used for testing are p-type Si wafers with relatively higher  $S$  than n-  
128 type Si.<sup>21</sup> One reason for choosing Si-based materials is that the band structure of Si is  
129 well known. Si-based devices are considered as an important thermoelectric materials,  
130 and often applied to a refrigeration systems, such as central processing units (CPUs) or  
131 field emission displays (FEDs).<sup>22</sup> We measured two p-type Si wafers manufactured by  
132 Sinyo Co.Ltd. and Shin-Etsu Chemical Co. with low and high carrier concentrations,  
133 respectively, although the exact concentration is unknown. Si wafers with a thickness of  
134 0.52 mm were cored into a disk shape with 2-mm diameter using an ultrasonic drilling  
135 machine.

136 A Kawai cell (6-8 type) was used for thermoelectric measurements under high  
137 pressure. The cell assembly is shown in Fig. 2. A Cr<sub>2</sub>O<sub>3</sub>-doped MgO octahedron with an  
138 edge-length of 14 mm was used as a pressure medium in second stage tungsten carbide  
139 anvils with a truncation edge length of 8 mm. The outer assemblage consisted of a  
140 Cr<sub>2</sub>O<sub>3</sub>-bearing MgO pressure medium, ZrO<sub>2</sub> thermal insulator, and a cylindrical MgO  
141 polycrystalline sleeve. Two TiB<sub>2</sub>-doped BN + AlN composite disk heaters with 4-mm  
142 diameter and 0.3-mm thickness were set at both sides of the sample using an MgO  
143 spacer. The electrodes of the sheet heater with two independent circuits were each

144 connected to the truncated WC anvil surface in the orthogonal direction. The disk-  
145 shaped sample was sandwiched by Mo electrodes. One sample face was covered by a  
146 Mo electrode, a  $W_{97}Re_3$ -  $W_{75}Re_{25}$  thermocouple (0.1 mm in diameter) for temperature  
147 reading, and one end of the W wire for probing the voltage difference placed at the  
148 center of the sample. The junction of the other  $W_{97}Re_3$ -  $W_{75}Re_{25}$  thermocouple and W  
149 wire were set on the opposite sample face. The other end of the W wires was connected  
150 to the truncation surface of the WC anvils located perpendicular to the sample surface.  
151 Outside the Kawai cell, six of the eight second-stage WC anvils were used as electrodes  
152 for monitoring the thermopower between both ends of the sample and dual heaters.  
153 These six second-stage anvils were connected to all six first-stage anvils, each of which  
154 was electrically insulated using Cu foil across the insulation plate. The two sets of  
155  $W_{97}Re_3$ - $W_{75}Re_{25}$  thermocouples were electrically insulated from the sheet heater by  
156 MgO and exited the cell through the pyrophyllite gaskets. The wires for monitoring  $T_1$ ,  
157  $T_2$ , and  $\Delta V$  were connected to a Keysight 34970A data logger.

158 High-pressure and high-temperature experiments were performed in a 6-axis  
159 multi-anvil apparatus. The 6-axis press has no guide blocks,<sup>23</sup> which allows sufficient  
160 space to handle the set of lead wires and minimize short circuits during compression.  
161 Each anvil of the 6-axis press is electrically insulated, which implies that even if four of  
162 the six surfaces are used for dual heating, the remaining two anvils can be used as  
163 electrodes for measuring emf. Reducing the numbers of probes through the gaskets is of  
164 great merit in multi-anvil experiments because wire breakage frequently occurs during  
165 compression.



166

### 167 **III. RESULTS AND DISCUSSION**

#### 168 **A. Dual heating**

169 To ensure accurate control of  $\Delta T$  between both ends of the sample, we tested the  
170 dual heating performance at 5 GPa by two approaches. In case (1), the temperature on  
171 one side of the sample ( $T_1$ ) was held fixed while the temperature on the other side ( $T_2$ )  
172 oscillated. In case (2), when  $T_1$  deviated from the target  $T$ ,  $T_2$  was simultaneously  
173 controlled in the opposite direction. The average  $T$  oscillates in the former case, whereas  
174 a constant average  $T$  can be maintained in the latter case. In this oscillation mode,  $\Delta T$   
175 values across the sample can be continuously adjusted from positive to negative. In both  
176 cases, a maximum peak-to-peak  $\Delta T$  of  $\pm 20$  K was applied.

177 Examples of temperature oscillations ( $\pm 20$  K) in high-temperature runs are shown  
178 in Fig. 3. The temperature fluctuation was controlled within 1 K of the set value at the  
179 two thermocouple junctions on both ends of the sample. For measurements at each  
180 temperature,  $\Delta T$  was produced around a given target temperature. The  $\Delta T$  could not be  
181 precisely controlled at  $T$  close to room temperature because the power required to  
182 generate  $\Delta T$  on both sides of the sample was too small compared with the original  $\Delta T$   
183 created by a single heater. However, a control of  $\Delta T$  was possible when the target  $T$  was  
184  $> 373$  K. Accurate control of the temperature becomes impossible at  $T > 1473$  K and the  
185 heater electrode frequently broke at  $T > 1500$  K. When both ends of the sample are held  
186 at the same temperature by dual heating, the power ( $W$ ) generated by each heater is  
187 equivalent. In case (1) where  $T_1$  is held fixed,  $W_2$  increases when  $T_2$  increases and  $W_1$

188 correspondingly decreases. In case (2),  $W_1$  and  $W_2$  showed the opposite behavior. In  
189 both cases, the total applied power remains nearly constant.

190

## 191 **B. Seebeck Coefficient measurement**

192 The Seebeck coefficient measurements of p-type Si wafers were performed over a  
193 temperature range of 473–1473 K at 100-K intervals at 3 and 5 GPa. The temperature  
194 dependence of the Seebeck coefficient of the bulk material was determined during both  
195 the heating and the cooling cycles. The sample environment in the cell assembly usually  
196 changes during heating, and electrical conductivity measurements of hydrous samples in  
197 a multi-anvil press have shown different paths along heating and cooling cycles owing  
198 to sample dehydration.<sup>24</sup> The reliability of obtained data can therefore be confirmed by  
199 overlapping the Seebeck coefficient measured during both heating and cooling.

200 Our results show a linear response of voltage to changes in  $\Delta T$  with the slope  
201 yielding the Seebeck coefficient (Fig. 4).  $\Delta V$  should ideally be zero, when  $\Delta T = 0$ .  
202 Although a small degree of voltage offset is observed, the extent is substantially smaller  
203 than  $\Delta V$  produced by small changes of  $\Delta T$ . The measured voltage includes not only the  
204 sample but also both electrical and thermal contacts to the sample and the  
205 instrumentation.

206 The Seebeck coefficient of heavily B-doped Si obtained under variable temperature  
207 and constant pressure is shown in Fig. 5. The thermopower measurements were carried  
208 out by maintaining a constant press load and varying the temperature. At fixed pressure  
209 (5 GPa), the Seebeck coefficient decreases slightly with increasing temperature between

210 473 and 873 K, and then abruptly decreases to zero with increasing temperature above  
211 973 K. Although the carrier concentration of this sample is unknown, the absolute  $S$   
212 value and  $T$ -dependence of Si are in excellent agreement with those of p-type Si with  
213 carrier densities on the order of  $10^{18}$ – $10^{19}$   $\text{cm}^{-3}$  measured at room pressure.<sup>25–27</sup> The sign  
214 of  $S$  changes from positive to negative at  $\sim 1273$  K, which is close to the melting  
215 temperature of Si at 5 GPa. Previous experimental studies on the melting curve of Si I  
216 (diamond structure) yield the following relation  $T$  (K) =  $-62.3 (1.4)P$  (GPa) + 1683.<sup>28–</sup>  
217 <sup>33</sup> At 5 GPa, the melting temperature of Si is calculated to be 1372 K. The temperature  
218 of the Seebeck coefficient polarity change is lower than the Si I melting temperature,  
219 and is therefore not considered to be caused by melting.

220 Figure 6 shows the Seebeck coefficients of B-doped Si with low carrier  
221 concentrations at 3 GPa and variable temperature up to 1273 K. The thermopowers  
222 were measured at two different press loads and variable temperature up to 1000 K. The  
223 Seebeck coefficient slightly decreases with increasing temperature, and then abruptly  
224 decreases to negative values over the temperature range of 473–573 K. Above 573 K,  
225 the Seebeck coefficient slightly decreases with increasing temperature. Electrical  
226 resistivity also decreases abruptly in the same temperature range (Fig. 7). This behavior  
227 is consistent with that of p-type Si with low carrier concentrations on the order of  $10^{14}$   
228  $\text{cm}^{-3}$  measured at room pressure,<sup>34</sup> which is consistent with the dopant carrier  
229 concentration ( $4.6 \times 10^{14}$   $\text{cm}^{-3}$ ) estimated from the measured electrical resistivity of this  
230 sample ( $29 \Omega \cdot \text{cm}$ ) at room temperature and 3 GPa.<sup>35</sup>

231 The results of measurements of Si with different levels of donor doping demonstrate

232 a negligible pressure effect on the thermoelectric properties of Si, and that carrier  
233 concentration influences the  $T$ -dependent Seebeck coefficient. The temperatures at  
234 which the Seebeck coefficient rapidly decreases, increases from 500 to 900 K with  
235 increasing carrier concentration from  $10^{14}$  to  $10^{19}$   $\text{cm}^{-3}$ . This trend agrees qualitatively  
236 with results from an ab initio calculations that show the thermopower reaches a  
237 maximum at an electron carrier concentration of  $\sim 10^{15}$   $\text{cm}^{-3}$  at 500 K, while the  
238 maximum at 900 K shifts to a higher dopant level of  $10^{18}$   $\text{cm}^{-3}$ .<sup>26</sup>

239 The Seebeck coefficient is the sum of the diffusive part and phonon drag part with  
240 the former dominating thermopower in heavily doped samples and the latter dominating  
241 that of pure Si.<sup>36</sup> However, the phonon drag effect only dominates at temperatures  
242 below 300 K. For low dopant level Si, the thermopower rapidly vanishes at a distinct  
243 temperature of  $\sim 500$  K. The drop off of the Seebeck coefficient appears at the  
244 approximate temperature range between extrinsic and intrinsic electrical resistivity.<sup>34</sup> At  
245 this temperature, the electronic transport enters the bipolar intrinsic regime (Fig. 6). At  
246 high charge carrier concentrations of about  $10^{18}$   $\text{cm}^{-3}$ , the intrinsic regime likely  
247 becomes dominant near the melting temperature. The thermopower for Si wafers in the  
248 intrinsic transport regime converges to small negative values for electrons at higher  
249 temperature. Because the band gap of semiconductors generally decreases with  
250 increasing temperature, the chemical potential moves toward the band edge with  
251 increasing temperature in the “extrinsic” region and enters the band gap in the  
252 “intrinsic” temperature region.<sup>37</sup> The observed drop off of the Seebeck coefficient over  
253 the investigated temperature range therefore indicates that the carrier concentration

254 increases at certain temperatures, from the doping concentrations to the intrinsic values.

255

#### 256 **IV. CONCLUSIONS**

257 We report a new technique to measure the Seebeck coefficient under high pressure  
258 and high temperature in a Kawai-type multi-anvil apparatus. We have developed a dual-  
259 heating system in the 6-axis press installed at the Institute for Planetary Materials of  
260 Okayama University. The dual-heating system can precisely control the temperature  
261 difference between the two ends of a sample up to 1473 K and at least 5 GPa. The  
262 resistivity and Seebeck coefficient of Si have been measured to evaluate the  
263 effectiveness of this method. The results are in good agreement with the previous results  
264 measured at ambient pressure, suggesting that the applied pressure effect does not  
265 greatly affect the thermoelectric properties of Si. This approach is reliable and simple  
266 with a high success rate and good reproducibility. This technique can be widely applied  
267 for investigating the thermoelectrical properties of not only thermoelectric materials and  
268 but also mantle and core materials in the Earth's interior.

269

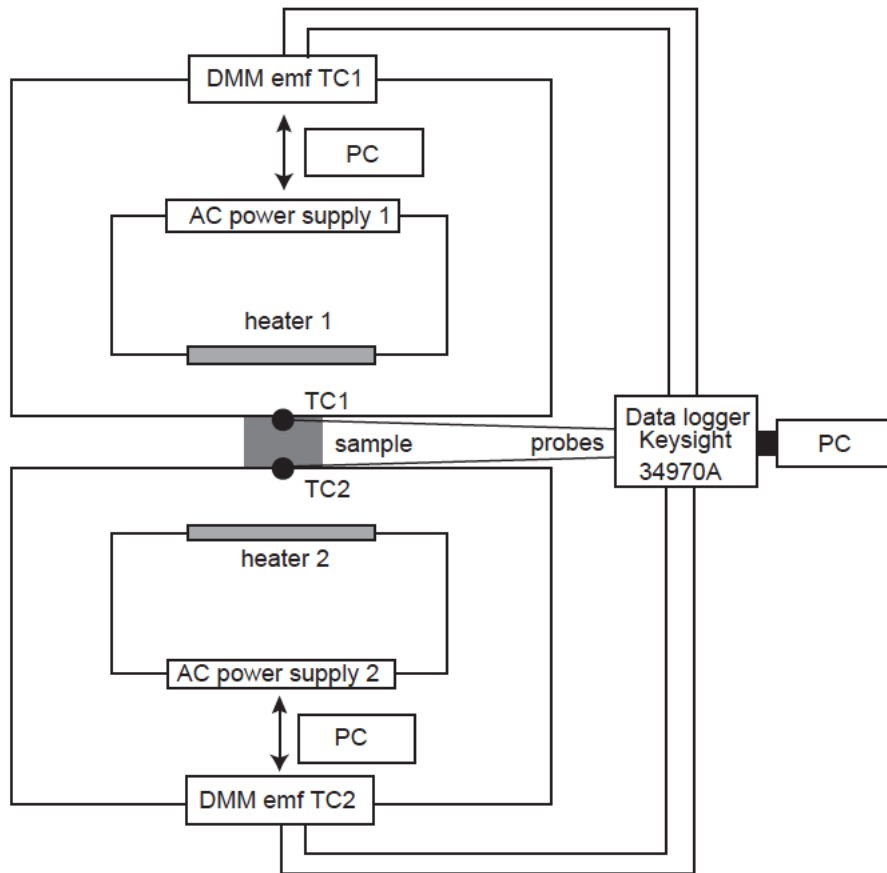
#### 270 **Acknowledgements**

271 We are grateful to D. Yamazaki, N. Tsujino, I. Ezenwa, N. Nakano for their insightful  
272 comments. We also thank two anonymous reviewers for their comments. This work was  
273 supported by the Ministry of Education, Culture, Sports, Science, and Technology of  
274 the Japanese Government, Grant Numbers, 15H05827 and 17H01155 to T.Y and  
275 17K06847 to Y. M.

276 References

- 277 <sup>1</sup>M. W. Schaefer and A. W. Webb, *Rev. Sci. Instrum.* 59, 2479 (1988).
- 278 <sup>2</sup>S. V. Ovsyannikov and V. V. Shchennikov, *Phys. Stat. Sol. B* 241(14), 3231–3234  
279 (2004).
- 280 <sup>3</sup>S. V. Ovsyannikov, V. V. Shchennikov, Y. S. Ponosov, S. V. Gudina et al., *J. Phys. D:*  
281 *Appl. Phys.* 37, 1151–1157 (2004).
- 282 <sup>4</sup>O. B. Tsiok, L. G. Khvostantsev, I. A. Smirnov, and A. V. Golubkov, *J. Exp. Theor.*  
283 *Phys.* 100, 752 (2005).
- 284 <sup>5</sup>N. V. Morozova, S. V. Ovsyannikov, I. V. Korobeinikov, A. E. Karkin, K. Takarabe,  
285 Y. Mori, S. Nakamura, and V. V. Shchennikov, *J. Appl. Phys.* 115, 213705 (2014).
- 286 <sup>6</sup>V. V. Shchennikov and S. V. Ovsyannikov, *Solid State Commun.* 126, 373 (2003).
- 287 <sup>7</sup>S. V. Ovsyannikov and V. V. Shchennikov, *Appl. Phys. Lett.* 90, 122103 (2007).
- 288 <sup>8</sup>B. Chen, Y. Li, and Z.-Y. Sun, *J. Electron. Mater.* 47, 3099 (2018).
- 289 <sup>9</sup>N. V. Morozova, I. V. Korobeinikov, S. V. Ovsyannikov, *J. Appl. Phys.* 125, 220901  
290 (2019).
- 291 <sup>10</sup>R. N. Schock, A. Duba, T. J. Shankland, *J. Geophys. Res.* 94, 5829–5839 (1989).
- 292 <sup>11</sup>S. Constable, J. J. Roberts, *Phys. Chem. Mineral.* 24, 319–325 (1997).
- 293 <sup>12</sup>V. V. Shchennikov, S. V. Ovsyannikov, A. Y. Derevskov, V. V. Shchennikov, Jr, *J.*  
294 *Phys. Chem. Sol.* 67, 2203–2209 (2006).
- 295 <sup>13</sup>S. V. Ovsyannikov, V. V. Shchennikov, G. V. Vorontsov, A. Y. Manakov et al., *J.*  
296 *Appl. Phys.* 104, 053713 (2008).
- 297 <sup>14</sup>V. V. Shchennikov, S. V. Ovsyannikov, G. V. Vorontsov, and V. V. Kulbachinskii, *J.*  
298 *Phys.: Conf. Ser.* 215, 012185 (2010).
- 299 <sup>15</sup>T. Yoshino, *Surv. Geophys.* 31, 163–206 (2010).
- 300 <sup>16</sup>M. Osako, E. Ito, A. Yoneda, *Phys. Earth Planet. Inter.* 143–144, 311–320 (2004).
- 301 <sup>17</sup>M. K. Jacobsen, W. Liu, and B. Li, *Rev. Sci. Instrum.* 83, 093903 (2012).
- 302 <sup>18</sup>B. Yuan, Q. Tao, X. Zhao, K. Cao, T. Cui, X. Wang, and P. Zhu, *Rev. Sci. Instrum.*  
303 85, 013904 (2014).
- 304 <sup>19</sup>J. Martin, T. Tritt, and C. Uher, *J. Appl. Phys.* 108, 121101 (2010).
- 305 <sup>20</sup>V. Ponnambalam, S. Lindsey, N. S. Hickman, and T. M. Tritt, *Rev. Sci. Instrum.* 77,  
306 073904 (2006).
- 307 <sup>21</sup>O. Yamashita, *J. Appl. Phys.* 95, 178–183 (2004).

308 <sup>22</sup>F. Salleh, K. Asai, A. Ishida, H. Ikeda, Appl. Phys. Exp. 2. 071203 (2009)  
309 <sup>23</sup>E. Ito, T. Katsura, D. Yamazaki, A. Yoneda, M. Tado, T. Ochi, E. Nishibara, A.  
310 Nakamura, Phys. Earth Planet. Inter., **174**, 264–269 (2009).  
311 <sup>24</sup>T. Yoshino, T. Matsuzaki, S. Yamashita, T. Katsura, Nature 443, 973–976 (2006).  
312 <sup>25</sup>A. Ohishi, X. Xie, Y. Miyazaki, Y. Aikebaier, H. Muta, K. Kurosaki, S. Yamanaka,  
313 N. Uchida, T. Tada, Jpn. J. Appl. Phys. 54, 071301 (2015).  
314 <sup>26</sup>N.F. Hinsche, I. Mertig, and P. Zahn, J. Phys. Condens. Matter 23, 295502 (2011).  
315 <sup>27</sup>A. Stranz, J. Kahler, A. Waag, and E. Peiner, J. Electron. Mater. 42, 2381 (2013).  
316 <sup>28</sup>A. Jayaraman, W. Klement, G.C. Kennedy, Phys. Rev. 130, 540 (1963).  
317 <sup>29</sup>F. P. Bundy, J. Chem. Phys. 41, 3809 (1964).  
318 <sup>30</sup>J. Lees, B.H.J. Williamson, Nature 208, 278 (1965).  
319 <sup>31</sup>V. V. Brazhkin, A. G. Lyapin, S. V. Popova, R. N. Voloshin, Phys. Rev. B 51, 7549  
320 (1995).  
321 <sup>32</sup>G. A. Voronin, C. Pantea, T. W. Zerda, L. Wang, Y. Zhao, Phys. Rev. B 68, 020102  
322 (2003).  
323 <sup>33</sup>A. Kubo, Y. Wang, C. E. Runge, T. Uchida, B. Kiefer, N. Nishiyama, T. S. Duffy, J.  
324 Phys. Chem. Solid. 69, 2255–2260 (2008).  
325 <sup>34</sup>T. H. Geballe and G. W. Hull, Phys. Rev. 98, 940 (1955).  
326 <sup>35</sup>G. Masetti, M. Severi, and S. Solmi, IEEE Transactions on Electron Devices, 30, 764  
327 (1983).  
328 <sup>36</sup>L. Weber and E. Gmelin: Appl. Phys. A 53, 136 (1991).  
329 <sup>37</sup>M. Akasaka, T. Iida, A. Matsumoto, K. Yamanaka, Y. Takanashi, T. Imai, and N.  
330 Hamada, J. Appl. Phys. 104, 013703 (2008)  
331  
332

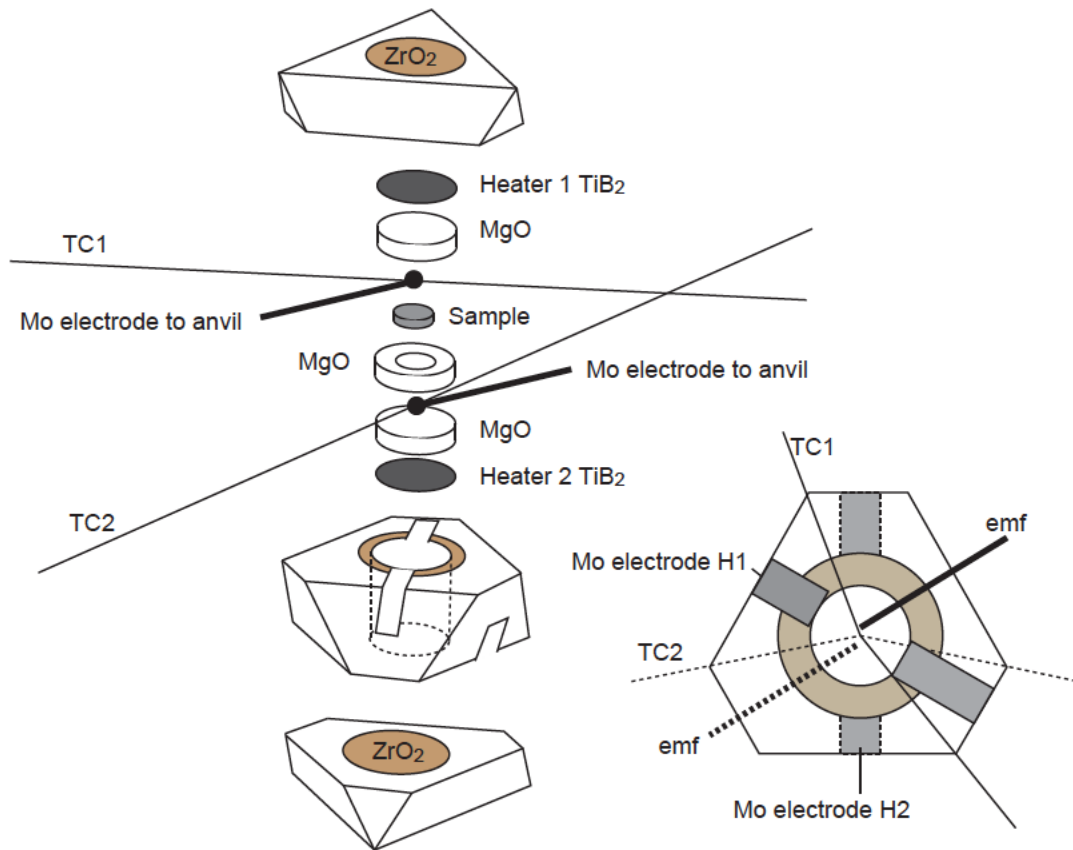


333

334 FIG. 1. Schematic drawing of the Seebeck coefficient and resistivity measurement setup  
 335 by dual heating in a Kawai-type multi-anvil apparatus. Temperatures at two ends of the  
 336 sample are monitored by two sets of thermocouples, and two resistive heaters are  
 337 separately computer-controlled. A data logger (Keysight 34970A) collects  $T_1$ ,  $T_2$  and  $\Delta V$   
 338 data as a function of time.

339





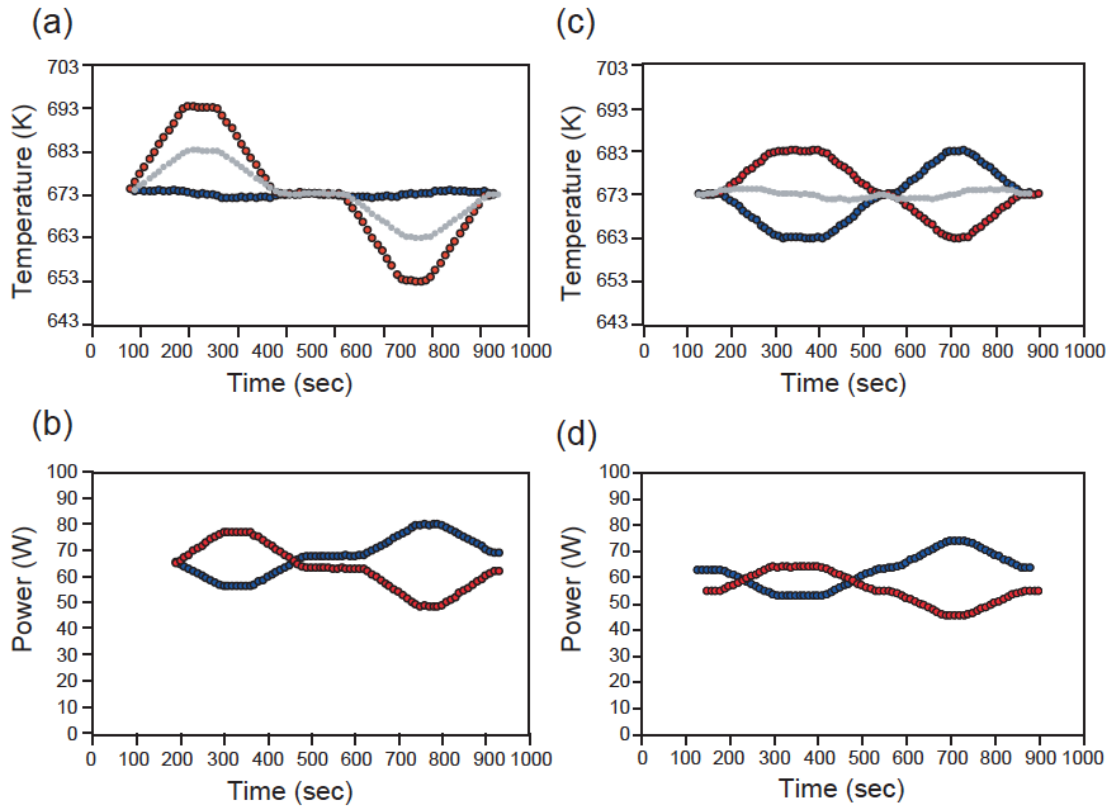
340

341 FIG. 2. Schematic illustration of the octahedron cell assembly used for the Seebeck  
 342 coefficient and resistivity measurements.

343

344

345

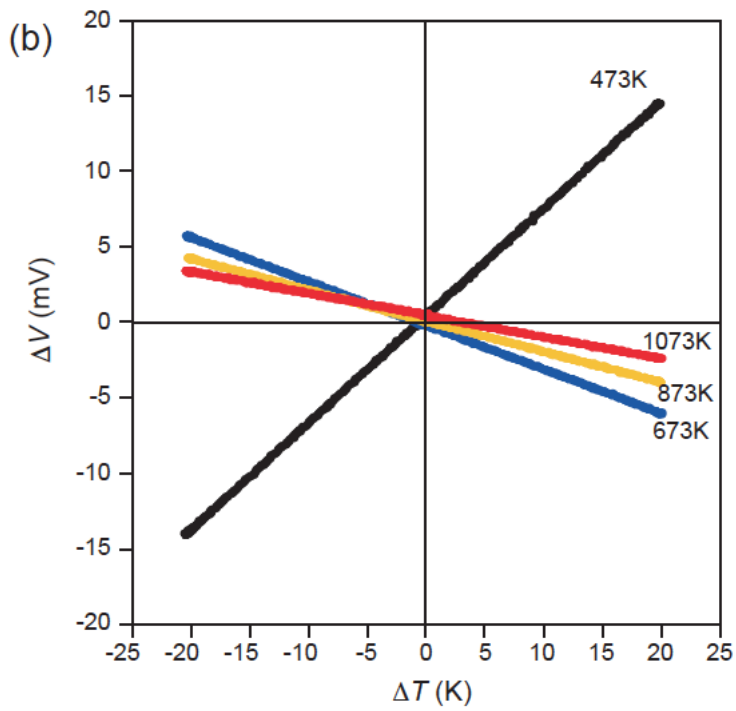
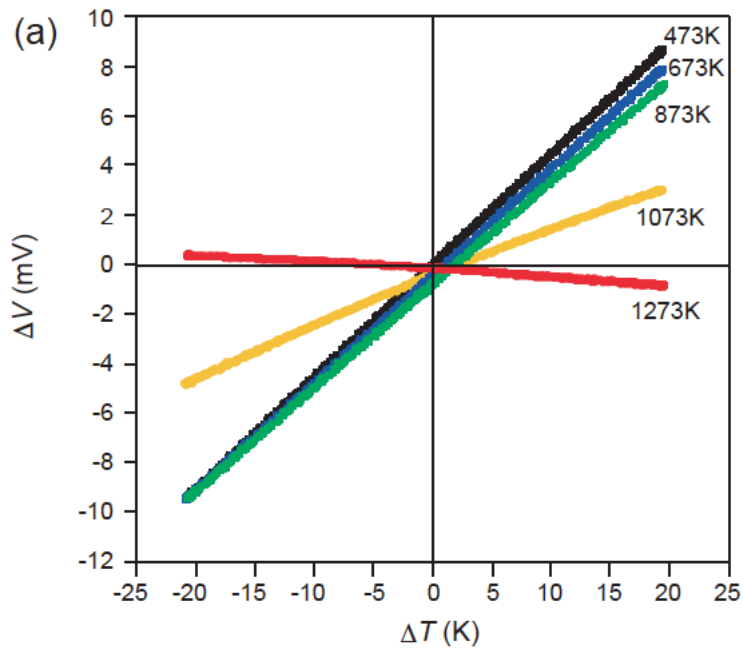


346

347 FIG. 3. Variations of temperature and heating power during the Seebeck coefficient  
 348 measurement at 673 K by dual heating for case 1 with the fixed  $T_1$  and case (2) where  
 349 the temperatures of  $T_1$  and  $T_2$  oscillate in opposite directions. The top, bottom, and  
 350 average temperature of the sample are shown as a function of time for (a) case 1 and (c)  
 351 case 2. Red, blue, and gray circles denote  $T_1$ ,  $T_2$ , and average temperature, respectively.

352 The applied power for heating at the top and bottom heaters is shown as a function of  
 353 time for (b) case 1 and (d) case 2. Red and blue circles denote applied powers  $W_1$  and  
 354  $W_2$  for heaters 1 and 2, respectively.

355



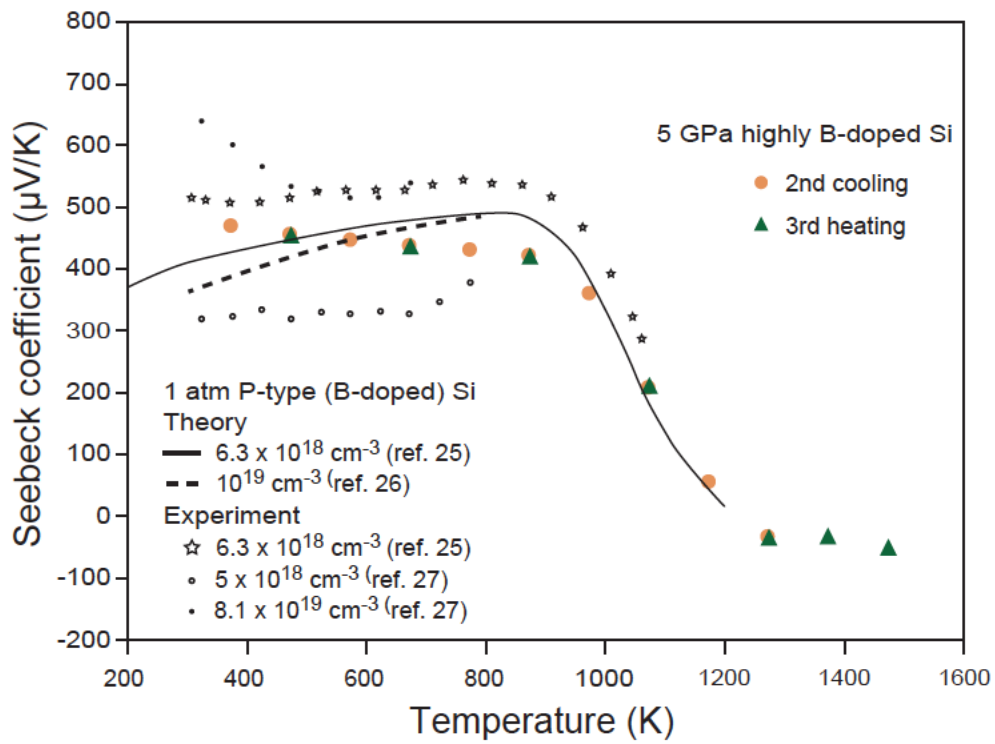
356

357 FIG. 4. Voltage response to the temperature difference ( $\Delta T$ ) for (a) the heavily B-doped

358 Si at 473, 673, 873, 1073, and 1273 K and (b) Si with low carrier concentration at 473,

359 673, 873, and 1073 K.

360



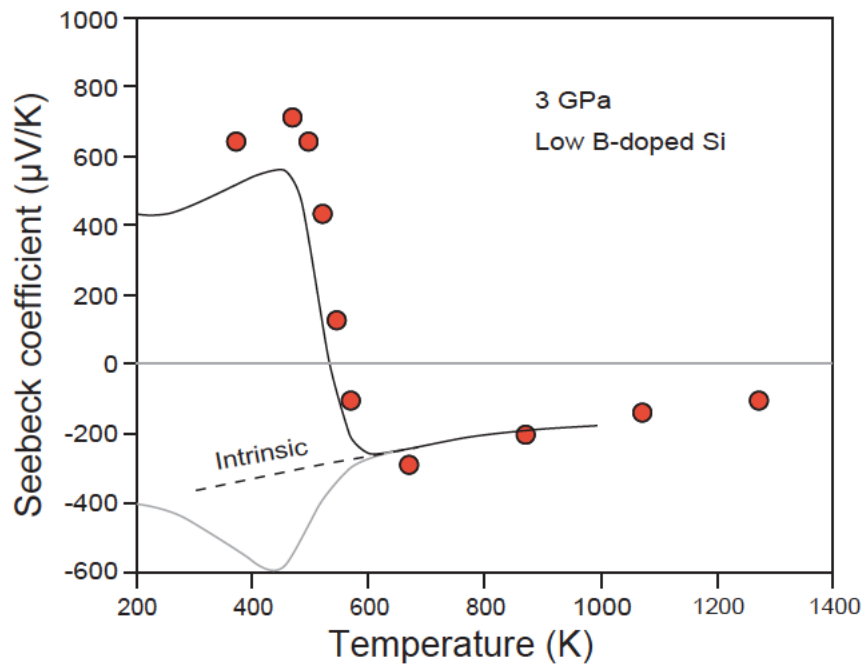
361

362 FIG 5. Temperature dependence of the Seebeck coefficient of p-type Si with high

363 carrier concentration at 5 GPa. Also shown are previously reported Seebeck coefficients

364 of Si with high carrier concentrations ( $10^{18-19} \text{ cm}^{-3}$ ).<sup>22-24</sup>

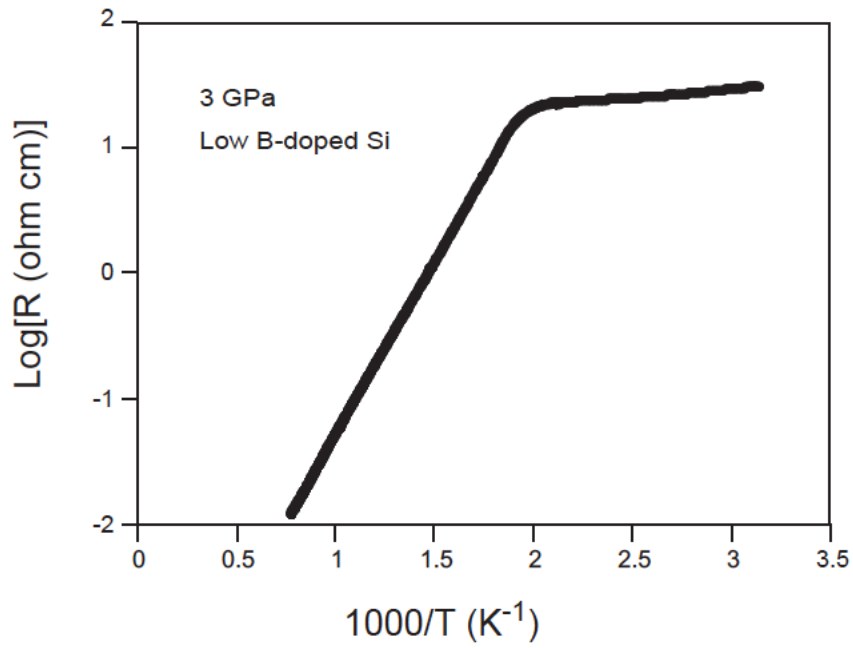
365



366

367 FIG. 6. Seebeck coefficient of p-type Si with low carrier concentration at 3 GPa as a  
 368 function of temperature. Solid and gray lines indicate calculated values<sup>31</sup> for p- and n-  
 369 type Si, respectively. The dashed line represents the calculated Seebeck coefficients for  
 370 the intrinsic regime<sup>31</sup>.

371



372

373 FIG. 7. Electrical resistivity of p-type Si with low carrier concentration at 3 GPa as a

374 function of reciprocal temperature.

375

